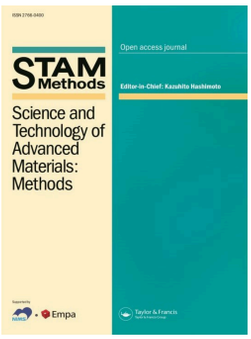

Science and Technology of Advanced Materials: Methods

ISSN: 2766-0400 (Online) Journal homepage: www.tandfonline.com/journals/tstm20

Creep data of Hastelloy X fabricated by laser powder bed fusion

Kota Sawada, Tomotaka Hatakeyama, Masahiro Kusano & Makoto Watanabe

To cite this article: Kota Sawada, Tomotaka Hatakeyama, Masahiro Kusano & Makoto Watanabe (2025) Creep data of Hastelloy X fabricated by laser powder bed fusion, Science and Technology of Advanced Materials: Methods, 5:1, 2582996, DOI: 10.1080/27660400.2025.2582996

To link to this article: https://doi.org/10.1080/27660400.2025.2582996

© 2025 The Author(s). Published by National Institute for Materials Science in partnership with Taylor & Francis Group

Published online: 20 Nov 2025.

Submit your article to this journal

View related articles

View Crossmark data

Full Terms & Conditions of access and use can be found at
https://www.tandfonline.com/action/journalInformation?journalCode=tstm20

SCIENCE AND TECHNOLOGY OF ADVANCED MATERIALS: METHODS
2025, VOL. 5, NO. 1, 2582996
https://doi.org/10.1080/27660400.2025.2582996

Taylor & Francis
Taylor & Francis Group

OPEN ACCESS Check for updates

Creep data of Hastelloy X fabricated by laser powder bed fusion

Kota Sawada, Tomotaka Hatakeyama, Masahiro Kusano and Makoto Watanabe

Research Center for Structural Materials, National Institute for Materials Science, Tsukuba, Ibaraki, Japan

ABSTRACT

The creep behavior of Hastelloy X fabricated by laser powder bed fusion was investigated, focusing on the testing temperatures of 700°C, 800°C, 900°C and 1000°C. Hastelloy X was selected as the first step because the Hastelloy X is a solid solution strengthened Ni-based alloy and a relatively simple material. For PiHA heat, the stress axis was parallel to the build direction, whereas for PiHC heat it was perpendicular. The creep strength of PiHA was similar to that of the conventional Hastelloy X at 700°C to 1000°C. The creep life of PiHC was one order of magnitude shorter than that of PiHA at 800°C and 900°C. For estimating allowable stress of additively manufactured Hastelloy X, the creep strength of PiHC will be minimum value. Therefore, the creep strength should be improved for PiHC to establish allowable stress comparable to the conventional Hastelloy X. The creep ductility was much lower in PiHA and PiHC than in the conventional Hastelloy X at all testing temperatures. No large difference in creep ductility was observed between PiHA and PiHC. Double local minimum values of creep rate were recognized in creep rate versus time curves at 700°C and 800°C for PiHA and PiHC. Creep voids and cracks were observed at grain boundaries perpendicular to the stress axis in PiHA and PiHC. $M_{23}C_6$, μ phase, R phase and M_6C particles were observed after creep exposure.

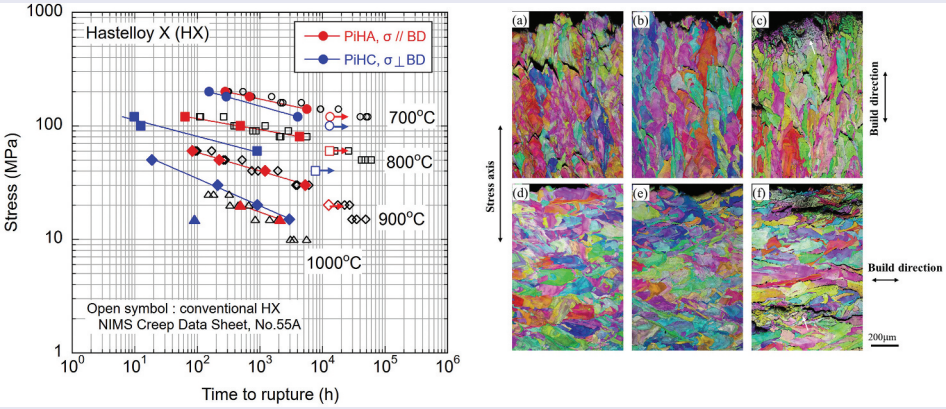

ARTICLE HISTORY
Received 5 August 2025
Revised 12 October 2025
Accepted 28 October 2025

KEYWORDS
Hastelloy X; additive manufacturing; creep strength; creep deformation behavior; precipitates

IMPACT STATEMENT

This paper shows systematic creep data for Hastelloy X fabricated by laser powder bed fusion. The creep strength of PiHA (stress axis//build direction) was similar to that of the conventional Hastelloy X at 700°C to 1000°C. The creep life of PiHC (stress axis ⊥ build direction) was one order of magnitude shorter than that of PiHA at 800°C and 900°C.

1. Introduction

The additive manufacturing (AM) technique allows a near-net shaping of complex products. For heat-resistant materials, many works have focused on AM of Ni-based alloys for aircraft engines and gas turbines [1–6]. In the case of heat-resistant steels, for example, creep properties of Modified 9Cr-1Mo steel and SUS316 steel fabricated by AM have been reported [7–10]. For the safety of components fabricated by AM, the long-term reliability of AM materials should be ensured, considering fatigue and creep behavior. The American Society of Mechanical Engineers (ASME) code actively standardizes materials fabricated by AM [11] and the Japan Society of Mechanical Engineers (JSME) has also started to develop a standard for AM materials [12]. For the standardization of heat-resistant materials fabricated by AM, long-term creep data should be systematically obtained. Furthermore, heat-to-heat variation of creep

CONTACT Kota Sawada sawada.kota@nims.go.jp Research Center for Structural Materials, National Institute for Materials Science, 1-2-1 Sengen, Tsukuba, Ibaraki 305-0047, Japan

© 2025 The Author(s). Published by National Institute for Materials Science in partnership with Taylor & Francis Group
This is an Open Access article distributed under the terms of the Creative Commons Attribution License (http://creativecommons.org/licenses/by/4.0/), which permits unrestricted use, distribution, and reproduction in any medium, provided the original work is properly cited. The terms on which this article has been published allow the posting of the Accepted Manuscript in a repository by the author(s) or with their consent.

strength should also be investigated to evaluate minimum creep strength and establish allowable stresses [13]. However, there are not enough creep data for AM materials for standardization compared with those for conventional heat-resistant materials.

For Ni-based alloys, a material strengthened by γ' and γ'' precipitates such as alloy 718 and IN738LC has good creep resistance. Therefore, many studies have examined these materials fabricated by AM [3–5,14]. Hastelloy X is known as a solid solution strengthened Ni-based alloy, although a carbide and intermetallic compound are formed after creep exposure [15]. To understand the comprehensive creep properties of Ni-based alloys fabricated by AM, a relatively simple material such as Hastelloy X should be selected as the first step. However, there are not enough systematic creep data for Hastelloy X fabricated by AM [16–18]. Accordingly, this study investigated the creep properties and microstructural changes for Hastelloy X fabricated by AM, at testing temperatures of 700°C, 800°C, 900°C and 1000°C.

2. Experimental procedures

The chemical composition of powder for fabrication by AM is listed in Table 1 together with the requirements of conventional Hastelloy X fabricated by hot rolling and forging. The chemical composition of the powder was in the range of requirements. The particle size of the powder was 15–45 μm. Laser powder bed fusion (LPBF) was used to manufacture bars with 15 mm diameter and 90 mm length, using a 3D printer (SLM 280, SLM Solutions). The laser power, scan speed, hatch distance, layer thickness and rotation angle were 300 W, 909 mm/s, 0.1 mm, 0.03 mm and 67 degree, respectively. A chessboard scanning strategy, with each square dimension of 5 mm × 5 mm, was employed. The laser scanned each island with a 90-degree rotation of the scan vector relative to its neighbors, which helped to reduce residual stress and improve microstructure homogeneity. No heat treatment was performed after building the bars. Tensile and creep specimens with gauge diameter of 6 mm and gauge length of 30 mm were longitudinally machined from the bars. For heat PiHA, the stress direction of tensile and creep testing was parallel to the build direction, whereas for heat PiHC it was perpendicular.

Tensile tests were performed at room temperature, 700°C, 800°C, 900°C and 1000°C in accordance with JIS G 0567 [19]. The nominal strain rate of the specimens was controlled to 5×10^{-5} s^{-1} up to about 1.0% proof stress and 1.25×10^{-3} s^{-1} beyond that. Creep tests were conducted at 700°C, 800°C, 900°C and 1000°C in accordance with JIS Z 2271 [20]. Creep strain – time data were obtained using single-type creep testing machines. The temperature was maintained to within ±3°C for 700°C, 800°C and 900°C, and ±4°C for 1000°C.

For microstructural observations, the sample was cut longitudinally parallel to the build direction, then embedded in hard resin, and then polished with emery paper and mechanically and chemically polished by colloidal silica. Scanning electron microscopy (SEM), electron backscattered diffraction (EBSD) and Vickers hardness tests were used for investigating gauge and grip portions of creep ruptured samples. Extracted residues obtained from these grip portions were analyzed by X-ray diffractometry (XRD) to identify precipitates formed during creep exposure.

3. Experimental results

3.1 Tensile properties

Figure 1 shows the 0.2% proof stress and tensile strength of PiHA and PiHC together with those of conventional Hastelloy X plate and bars [21]. The 0.2% proof stress was clearly higher in PiHA and PiHC than in conventional materials up to 800°C. However, no large difference of 0.2% proof stress was observed between PiHA, PiHC, and the conventional materials at 900°C and 1000°C. There was no clear difference in tensile strength between PiHA and

Table 1. Chemical compositions of powder for fabrication by AM.

	Chemical composition (mass percent)							
	C	Si	Mn	P	S	Ni	Cr	Mo
Require-ment[1)]	0.05–0.15	≤ 1.0	≤ 1.0	≤ 0.040	≤ 0.030	bal.[4)]	20.5–23.0	8.0–10.0
ASME code [2), 3)]	0.05–0.15	≤ 1.0	≤ 1.0	≤ 0.04	≤ 0.03	bal.[4)]	20.5–23.0	8.0–10.0
PiHA	0.05	< 0.1	< 0.0	< 0.002	0.002	bal.[4)]	21.8	8.9
PiHC								
	W	Co	Ti	Al	B	N	Fe	O
Require-ment[1)]	0.2–1.0	0.5–2.5			≤ 0.010		17.0–20.0	
ASME code [2), 3)]	0.2–1.0	0.5–2.5					17.0–20.0	
PiHA	0.5	1.6	< 0.01	0.09	< 0.002	0.006	18.6	0.018
PiHC								

1) NW6002, JIS H 4551-2000, "Nickel and nickel alloy plate, sheet and strip", JIS H 4553-1999, "Nickel and nickel alloy bars"
2) ASME SB-435, 2021. Specification for UNS N06002, UNS N06230, UNS N12160, AND UNS R30556 PLATE, SHEET, AND STRIP
3) ASME SB-572, 2021. SPECIFICATION FOR UNS N06002, UNS N06230, UNS N12160, AND UNS R30556 ROD
4) balance

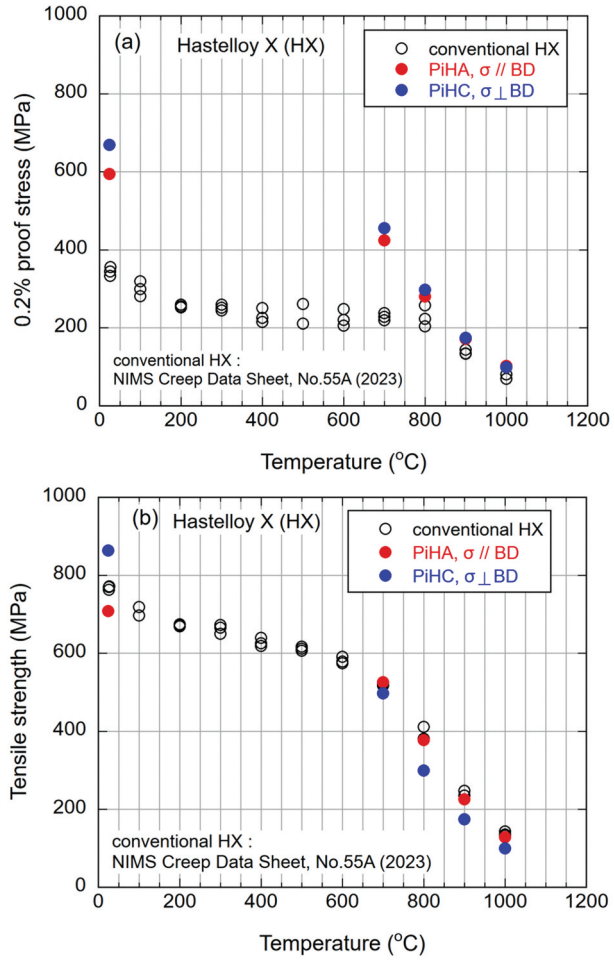

Figure 1. Relationship Between tensile property and temperature for PiHA and PiHC.(a)0.2% proof stress (b) tensile strength σ: stress axis BD : build direction

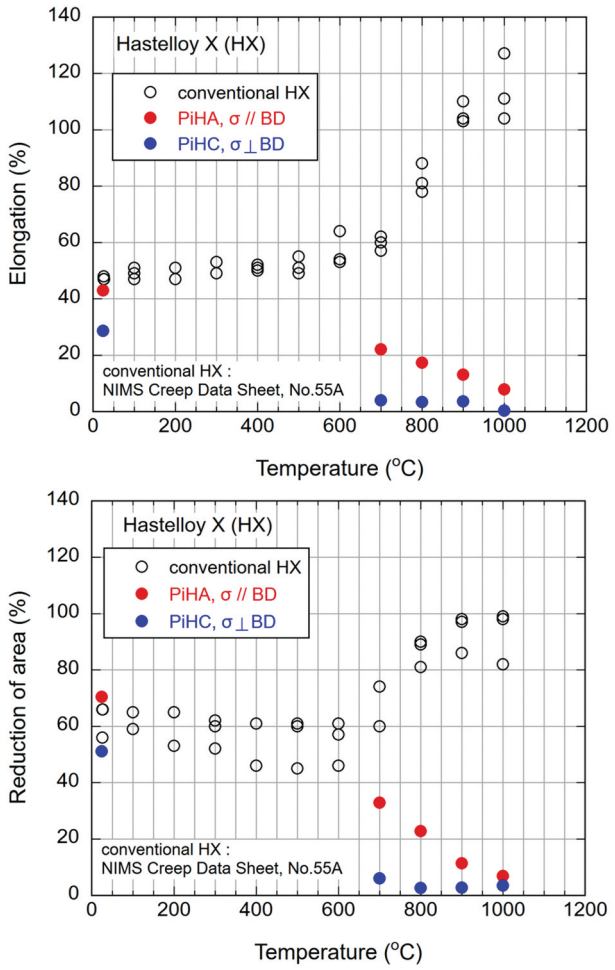

Figure 2. Relationship between tensile ductility and temperature for PiHA and PiHC. σ : stress axis BD : build direction

the conventional materials. The tensile strength of PiHC was lower than those of the conventional materials at 700°C to 1000°C although it was higher at room temperature.

Figure 2 shows relationships between tensile ductility and temperature. The tensile ductility increases with increasing temperature at higher than 600°C for the conventional materials while the ductility of PiHA and PiHC decreases with increasing temperature. At room temperature, the elongation and reduction of area for PiHA and PiHC were similar to those of the conventional materials, whereas they were clearly lower at 700°C to 1000°C. The tensile ductility was higher in PiHA than in PiHC at all testing temperatures, indicating that the ductility is improved when the stress direction is parallel to the build direction. There was no large difference between the material studied and the data in the tensile strength – elongation map at room temperature reported in the literature [22].

3.2 Creep properties

Figure 3 shows the stress versus time to rupture curve at 700°C to 1000°C together with the data of

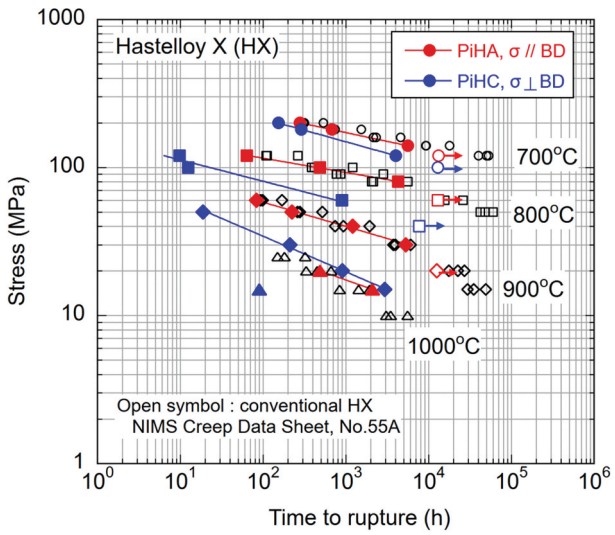

Figure 3. Stress versus time to rupture curve at 700°C to 1000°C for PiHA and PiHC. Arrows indicate on-going tests. σ: stress axis BD : build direction.

the conventional materials [23]. The creep strength of PiHA was similar to those of the conventional materials at 700°C to 1000°C. On the other hand, the creep strength was clearly lower in PiHC than in PiHA and the conventional materials. At 800°C

and 900°C, the creep life of PiHC was one order of magnitude shorter than that of PiHA. The value of the slope of stress versus time to rupture curve was larger in PiHC than in PiHA at 700°C to 900°C, indicating that the difference in creep life between PiHA and PiHC will be large in the long term. As shown in Figure 1, the 0.2% proof stress of PiHC is clearly higher than those of the conventional materials at 800°C and 900°C. However, the creep strength of PiHC is very low compared with those of the conventional materials at 800°C and 900°C, indicating that the 0.2% proof stress is not enough for evaluating the high-temperature strength of AM materials.

Creep ductility at 700°C to 1000°C are shown in Figure 4 and Figure 5. The elongation and reduction of area for PiHA and PiHC were much lower than those of the conventional materials at 700°C to 1000°C. The difference in ductility will be small among PiHA, PiHC and the conventional materials in the long term because the ductility of the conventional materials decreases with increasing time to rupture. There was no large difference in creep ductility between PiHA and PiHC. As shown in Figure 3, for AM Hastelloy X, improving creep strength, especially when stress is applied perpendicular to the build direction, is crucial at all testing temperatures. Figures 6 and 7 show relationships between creep rate and time at 700°C to 900°C for PiHA and PiHC, respectively. The creep rate basically decreased with increasing time and then increased after reaching the minimum creep rate at all testing temperatures. For PiHA, double local minimum values of creep rate were recognized under 140 MPa at 700°C and under 60 MPa at 800°C. The same behavior was observed under 100 MPa at 700°C for PiHC. It has been reported that the recovery of dislocation structures and the precipitation of carbides at grain boundaries during creep exposure are related to the occurrence of double local minimum values of creep rate in austenitic stainless steels [24]. Precipitation behavior will be discussed later. On the other hand, no double local minimum values of creep rate were observed at 900°C for PiHA and PiHC. Creep rate versus time curves under 30 MPa at 900°C are shown in Figure 8. The minimum creep rate of PiHA is one order of magnitude smaller than that of PiHC in the same way as creep life shown in Figure 3, although the creep rate of PiHA is almost the same as that of PiHC at the beginning of creep deformation.

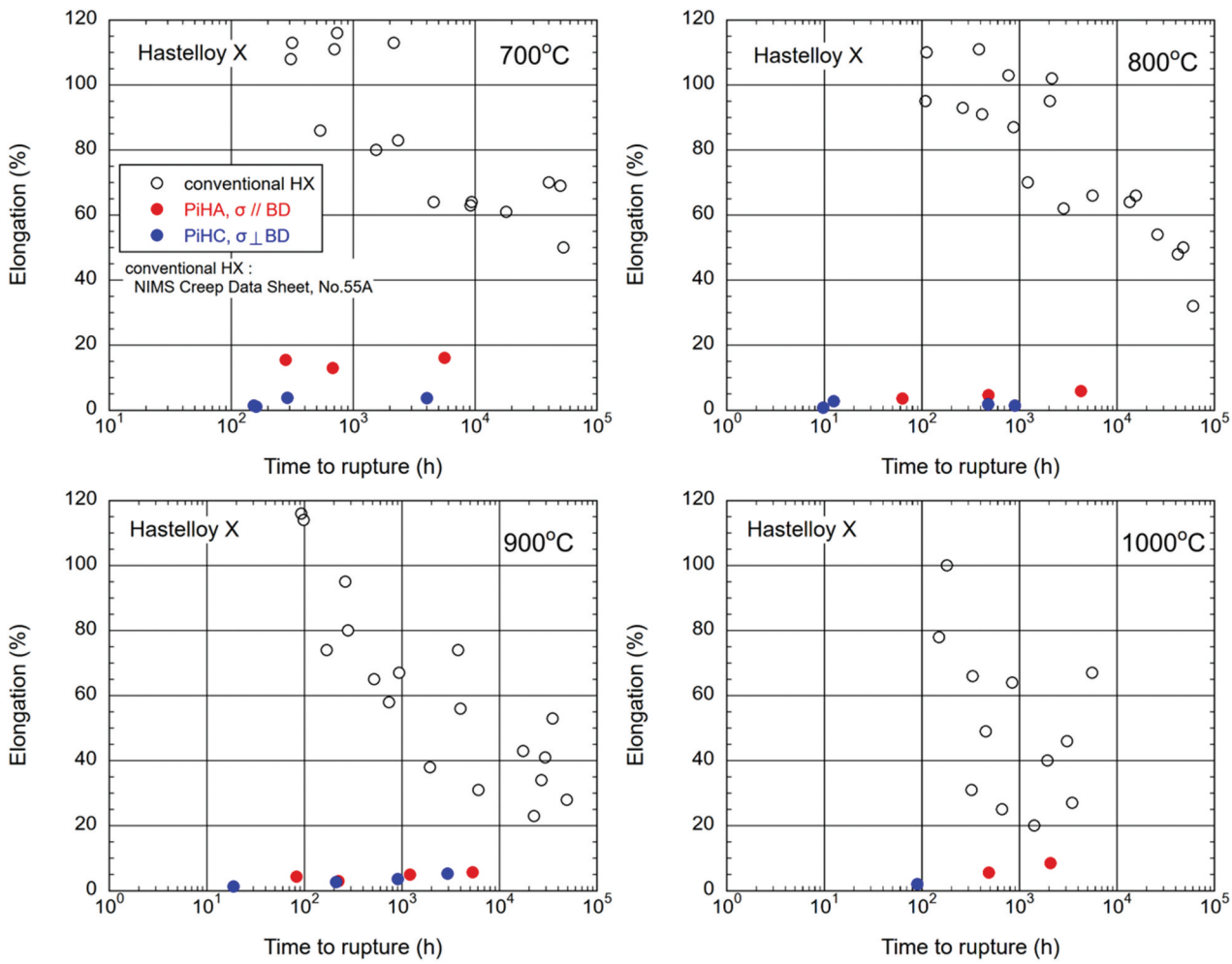

Figure 4. Relationship between elongation and time to rupture at 700°C to 1000°C for PiHC. σ: stress axis BD : build direction.

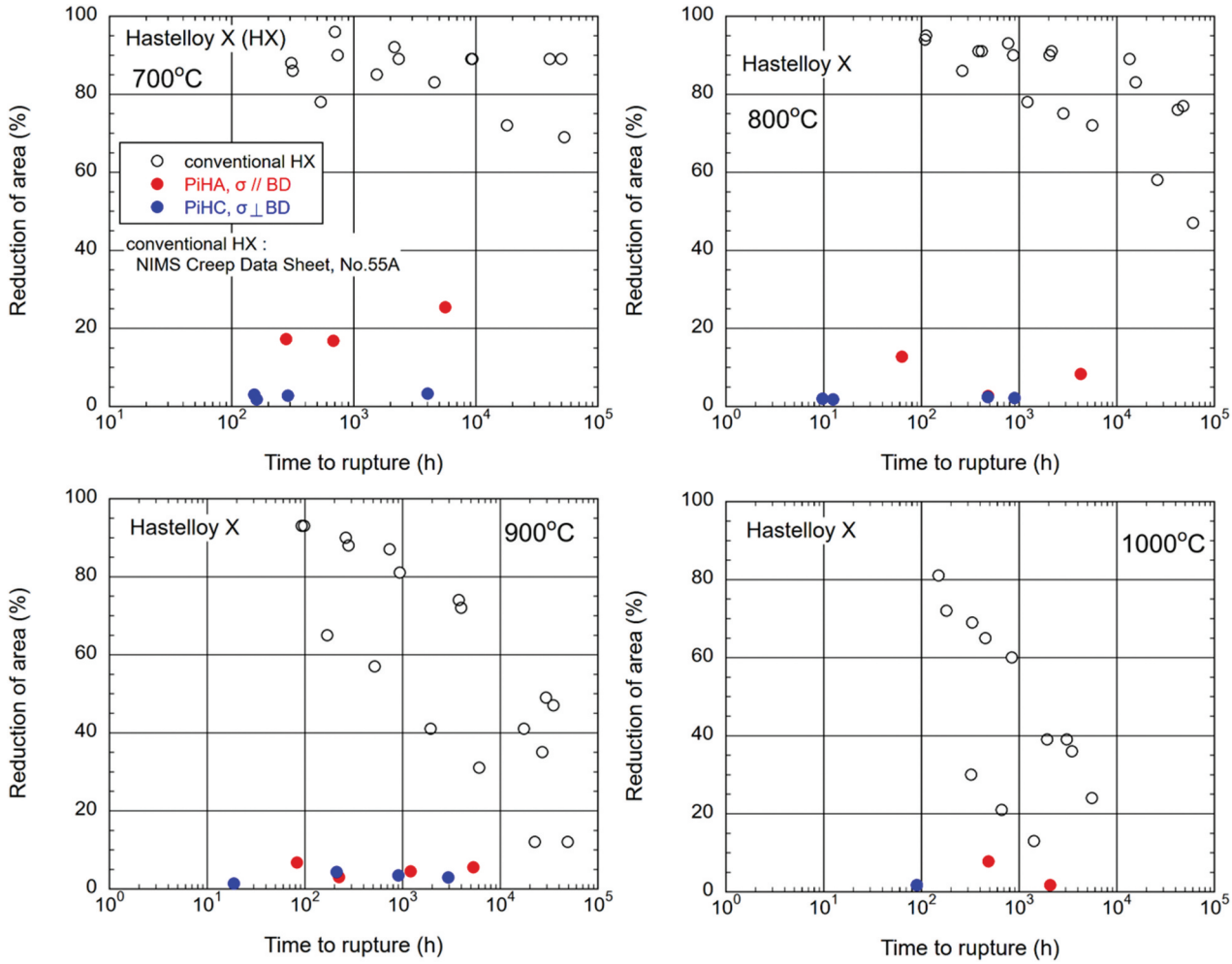

Figure 5. Relationship between reduction of area and time to rupture at 700°C to 1000°C for PiHA and PiHc. σ : stress axis BD : build direction.

Figure 9 shows the relationship between minimum creep rate and stress at 700°C to 1000°C together with those of the conventional materials. The minimum creep rate of PiHA was basically lower than those of the conventional materials under the same stress at all testing temperatures. For PiHC, the minimum creep rate was higher than those of the conventional materials at 900°C while there was no large difference at 700°C and 800°C. The minimum creep rate of PiHA was lower than that of PiHC at all testing temperatures. This is consistent with the difference in creep life shown in Figure 3.

The relationship between minimum creep rate and time to rupture is shown in Figure 10 together with the data of the conventional materials [23]. The Monkman – Grant rule was recognized for the conventional materials. However, the data of PiHA and PiHC disagree with the rule of the conventional materials; the time to rupture of PiHA and PiHC is always shorter than those of the conventional materials at the same minimum creep rate. The low creep ductility of PiHA and PiHC may cause the shorter time to rupture as shown in Figures 4 and 5.

3.3 Microstructural observation

Figures 11 and 12 show SEM micrographs of creep ruptured specimens for PiHA and PiHC, respectively. Creep voids and cracks were clearly observed for PiHA at all testing temperatures. The creep cracks tend to form at the grain boundaries perpendicular to the stress axis. For PiHC, no creep cracks and voids were confirmed at 700°C and 800°C although many cracks were formed at grain boundaries at 900°C. At 900°C, creep cracks propagate linearly along the build direction for PiHC while crack propagation occurs in a zigzag manner along the direction perpendicular to the stress axis for PiHA. The zigzag propagation of cracks is also observed after high-temperature fatigue [25]. This indicates that the crack propagation will be faster in PiHC than in PiHA. The difference of creep strength between PiHA and PiHC may be attributed to the difference of crack propagation behavior. If the grain boundary of PiHC becomes zigzag shape due to AM process optimization, the creep life of PiHC may be improved.

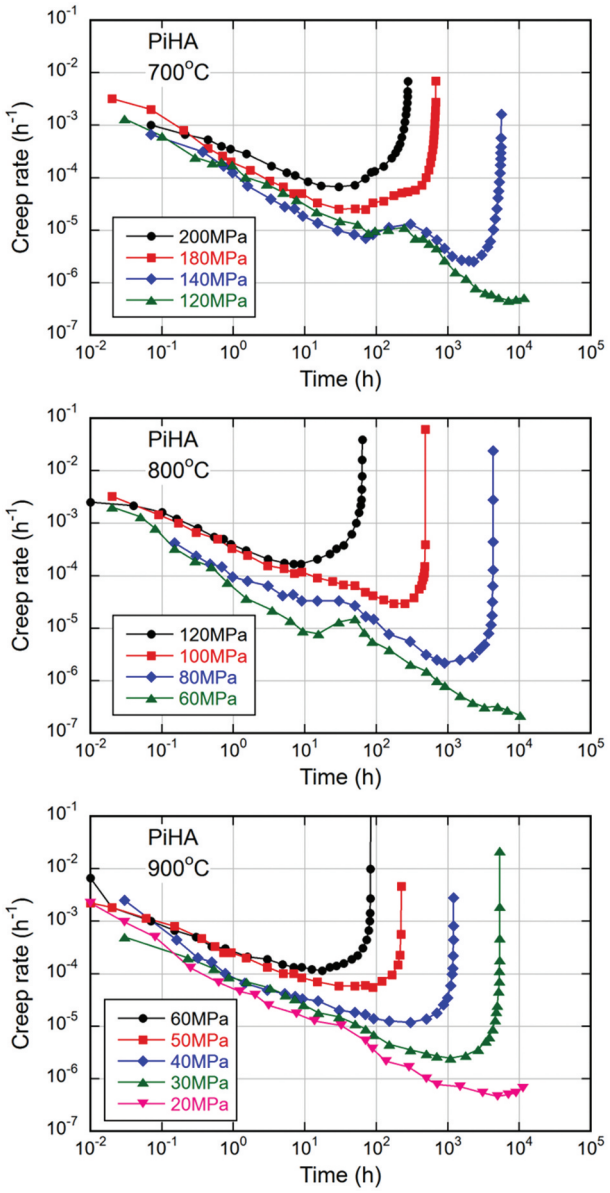

Figure 6. Creep rate versus time at 700°C to 900°C for PiHA. 700C-120MPa, 800°C-60MPa and 900C-20MPa are on-going tests.

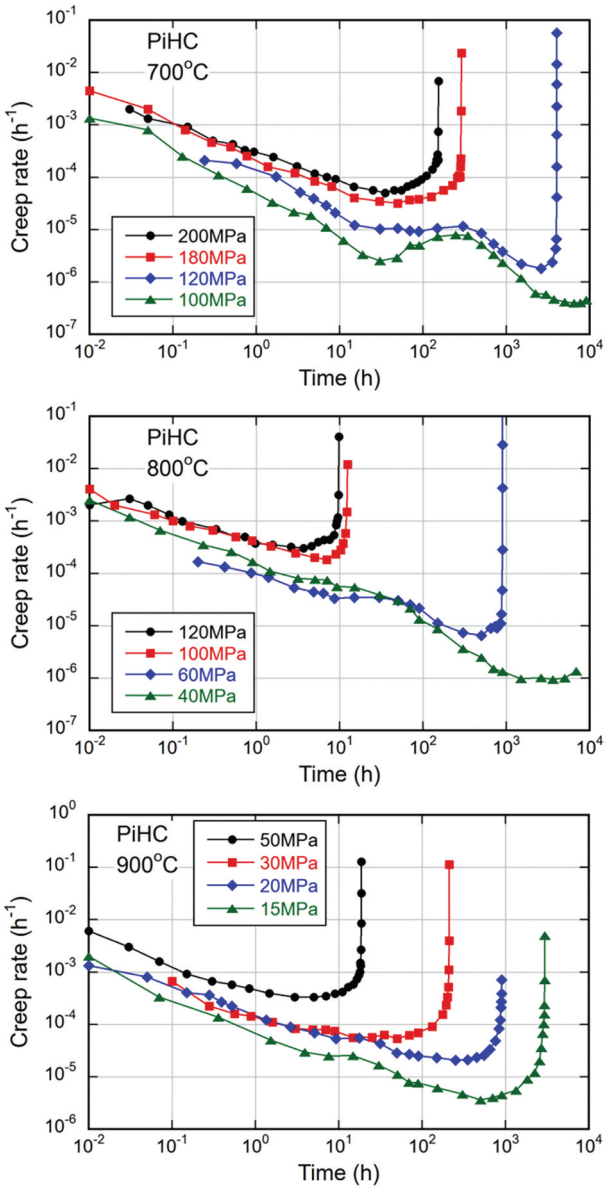

Figure 7. Creep rate versus time curve at 700°C to 900°C for PiHC. 700°C-100MPa and 800°C-40MPa are on-going tests.

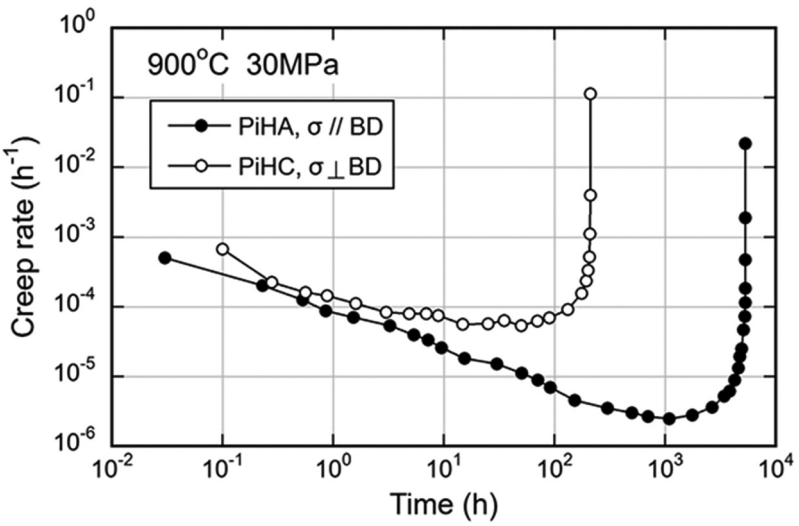

Figure 8. Creep rate versus time curve at 900°C under 30MPa for PiHA and PiHC. σ : stress axis BD : build direction.

SEM micrographs in gauge portions of creep ruptured specimens of PiHA are shown in Figure 13 at high magnification. It seems that creep voids initiated around large precipitates at grain boundaries. The precipitates formed during creep exposure because no precipitates were observed for as built condition of PiHA as shown in Figure 14. A similar behavior was recognized for austenitic stainless steel in which creep voids were formed around the σ phase at grain boundaries [26].

Figure 15 shows the inverse pole figure (IPF) map overlaid on the image quality (IQ) map by SEM-EBSD for creep ruptured specimens. At 700°C to 900°C, creep voids and cracks were clearly observed at grain boundaries for PiHA. For PiHC, fine creep voids were formed at grain boundaries at 700°C and 800°C although creep cracks were observed at grain boundaries at 900°C. Fine particles in Black and gray were recognized near creep cracks for both PiHA and PiHC at 900°C. It was confirmed by SEM-EDS that the particles were Cr- and O-rich, indicating chromium oxide may be formed by internal oxidation. Chromium oxide was not clear at 700°C and 800°C because of the lower temperature.

Figure 16 shows the results of XRD analysis for the extracted residue of grip portions of creep ruptured specimens for PiHA. At 700°C and 800°C, μ phase and $M_{23}C_6$ carbide were detected after creep rupture. In addition to these phases, R phase and M_6C carbide were also confirmed at 900°C. Precipitation of the R phase at 950°C was reported in AM Hastelloy X [27]. These precipitates were formed during creep exposure because no precipitates were observed for as-built samples as shown in Figure 14. Results of elemental maps by SEM-EDS for the gauge portions of creep ruptured specimens for PiHA are shown in Figure 17. Mo-rich and Cr-rich particles were observed at 700°C to 900°C. It was reported for conventional Hastelloy X that μ phase (Fe_7Mo_6) and $M_{23}C_6$ were observed after aging [15]. Therefore, the Mo-rich particles observed at 700°C and 800°C in Figure 17 are μ phase. The Cr-rich particles at 700°C and 800°C in Figure 17 are $M_{23}C_6$ because the M atom is normally Cr and Fe for $M_{23}C_6$. It seems that relatively large μ phase and $M_{23}C_6$ carbide are located at grain boundaries at 700°C and 800°C. At 900°C, it is difficult to distinguish R phase (Fe_3Mo_2) and M_6C (Mo_3Fe_3C) from μ phase because of the similarity of constituent elements on the elemental map. μ phase, R phase and M_6C are visible in Mo maps at 900°C in Figure 17. The size of the Mo-rich and Cr-rich particles increases with increasing testing temperature as shown in Figure 17. The same precipitation behavior was confirmed for PiHC in elemental maps, indicating that the build direction does not affect the precipitation behavior.

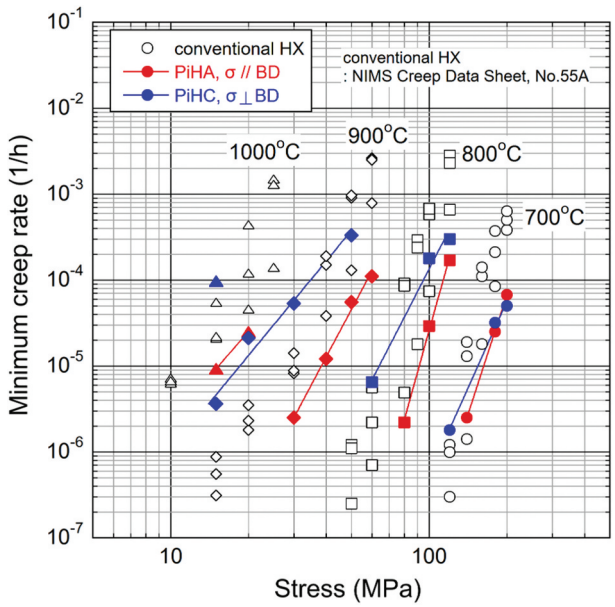

Figure 9. Relationship between stress and minimum creep rate at 700°C to 1000°C for PiHA and PiHC. σ : stress axis BD : build direction.

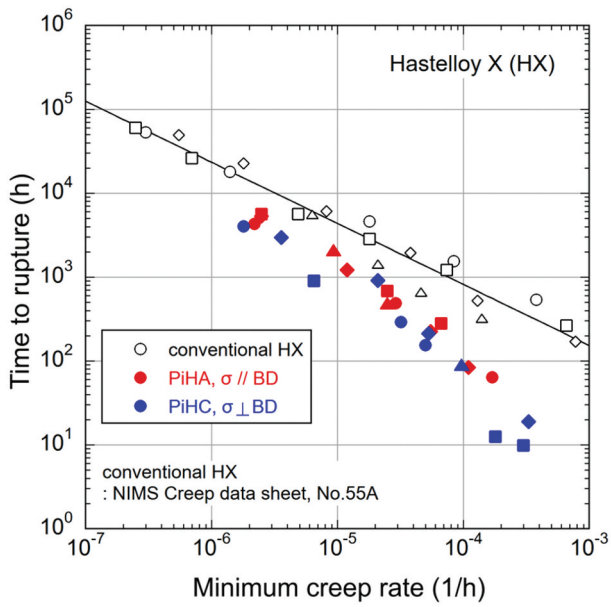

Figure 10. Relationship between minimum creep rate and time to rupture at 700°C to 1000°C for PiHA and PiHC. σ : stress axis BD : build direction.

3.4 Creep deformation behavior and microstructural change

Double local minimum values of creep rate were observed at 700°C and 800°C as shown in Figures 6 and 7. For PiHA, elemental maps were obtained from the grip portions of creep ruptured specimens to

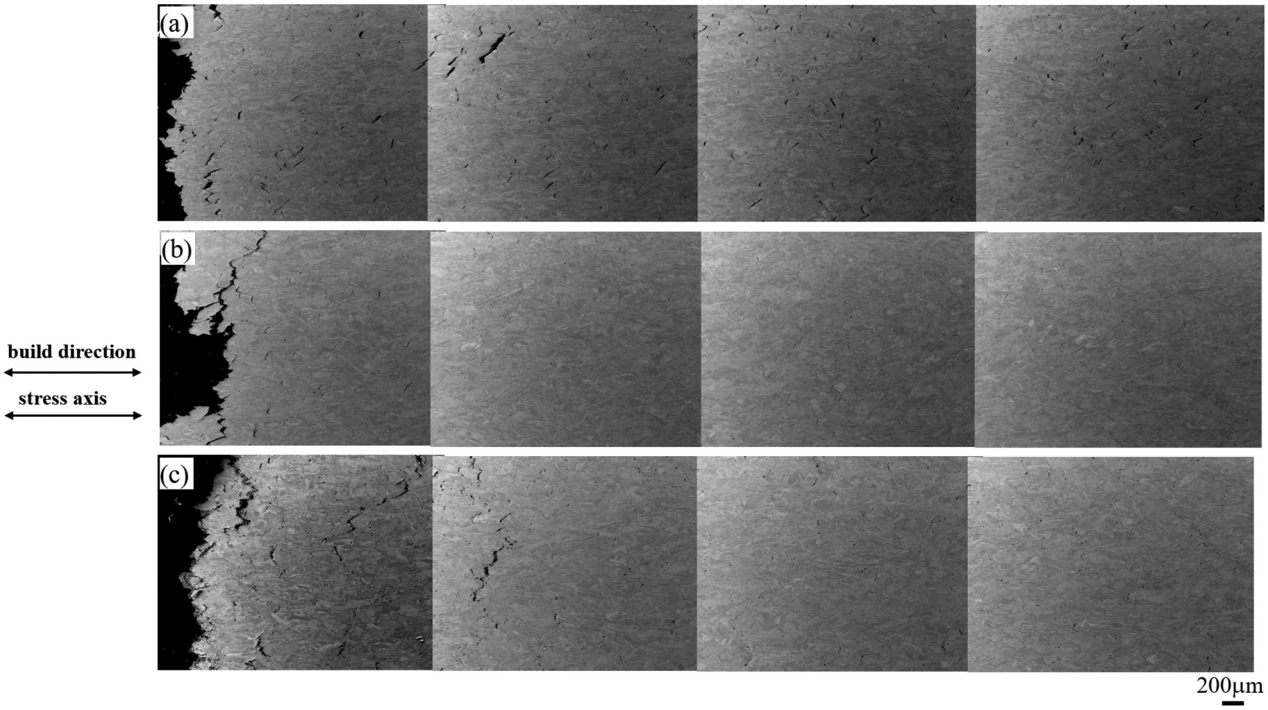

Figure 11. SEM micrographs of creep ruptured specimens of PiHA. (a)PiHA 700°C .140MPa tr=5612.4h, (b) PiHA 800°C . 80MPa tr=4288.9h, (c) PiHA 900°C . 30MPa tr=5319.3h.

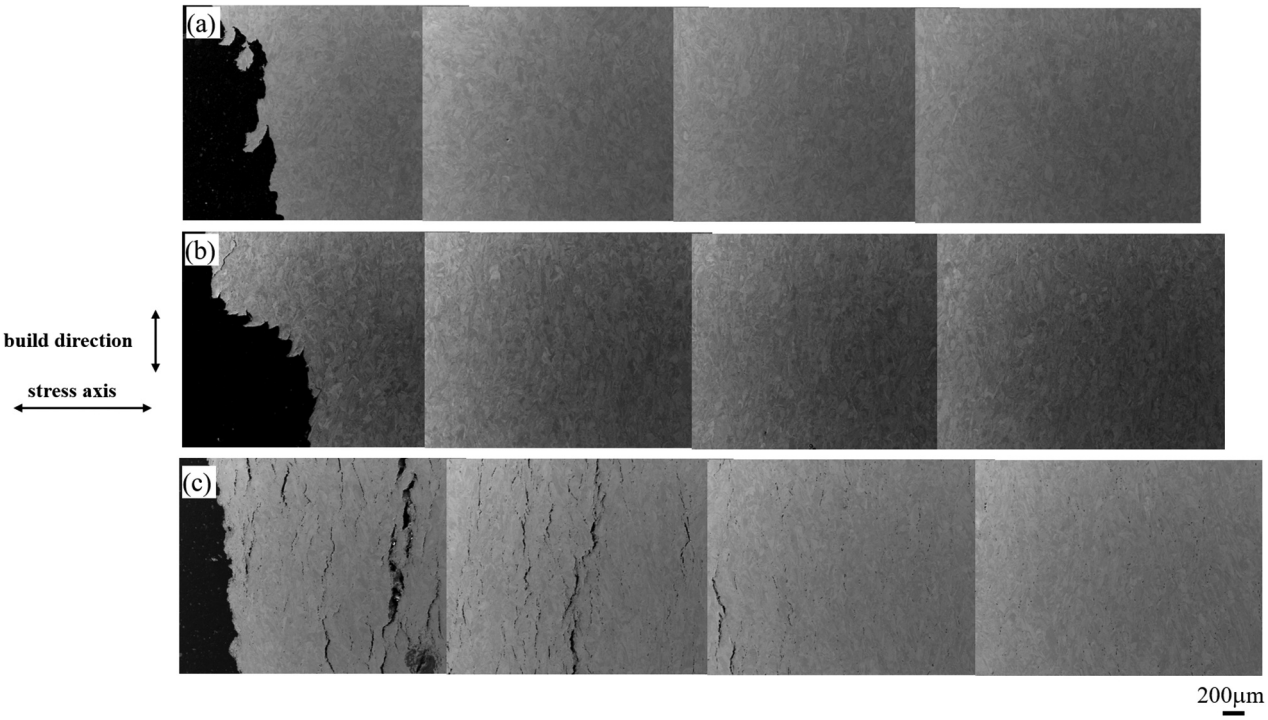

Figure 12. SEM micrographs of creep ruptured specimens of PiHC. (a)PiHC 700°C .120MPa tr=4030.2h, (b) PiHC 800°C . 60MPa tr=4288.9h, (c) PiHC 900°C . 15MPa tr=2949.5h.

clarify the relationship between precipitation behavior and the double local minimum creep rate as shown in Figure 18. At 700°C, μ phase and $M_{23}C_6$ particles were already formed by 279.8 h. The creep rate started to decrease for around 300 h after reaching the first local minimum value of creep rate at 700°C under 140 MPa of PiHA as shown in Figure 6. This indicates that the formation of μ phase and $M_{23}C_6$ particles during creep exposure contributes to the decrease in the creep rate after the first local minimum value at 700°C. At 800°C, many precipitates were already seen for 63.6 h. For PiHA, the decrease in creep rate after the first local minimum value of creep rate occurs for around 50 h at 800°C under 60 MPa as shown in Figure 6. The precipitation causes the decrease in creep rate in the same way as at 700°C. The same effect of precipitation

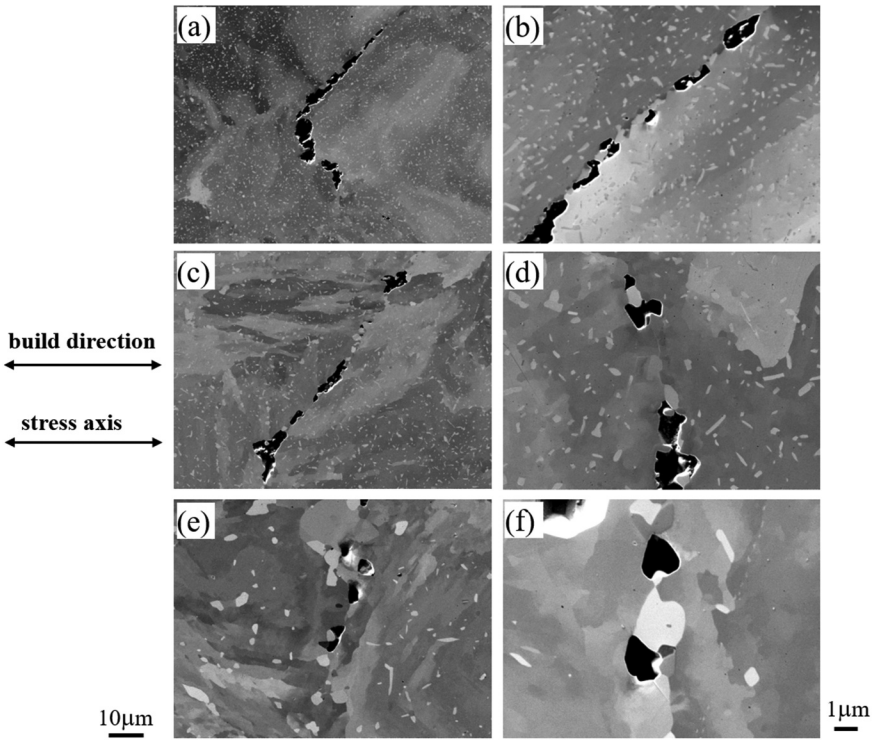

Figure 13. SEM micrographs around grain boundaries of creep ruptured specimens. (a),(b) PiHA 700°C . 140MPa tr=5612.4h (c),(d) PiHA 800°C . 80MPa tr=4288.9h (e),(f) PiHA 900°C . 30MPa tr=5319.3h.

Figure 14. SEM micrograph for as-built condition of PiHA.

during creep exposure on the decrease in creep rate after the first local minimum value of creep rate was observed at 700°C and 800°C for PiHC. At 900°C, the double local minimum values of creep rate may not be clearly seen as shown in Figure 6 because precipitation during creep exposure is very fast due to high temperature. It was reported for austenitic stainless steel [28] that no double local minimum values of creep rate were observed at 650°C and above while the double local minimum values were clearly seen at 600°C. Furthermore, no double local minimum values of creep rate were observed for austenitic stainless steel when pre-aging was performed before creep [29]. For AM materials, deformation twin and change of cell structure [30] can also affect double local minimum values of creep rate. However, creep tests should be interrupted for time corresponding to occurrence of double local minimum creep rate to make clear how change of deformation twin and cell structure affect double local minimum creep rate.

Vickers hardness was measured for the grip and gauge portions of creep ruptured specimens as shown in Figure 19. At 700°C for PiHA and PiHC, the hardness of the grip and gauge portions of creep ruptured specimens was higher than that of the as-built condition (before creep). On the other hand, the hardness tended to be low after creep rupture as compared to the as-built condition at 800°C and 900°C. Dislocations introduced during manufacturing and creep deformation and precipitation can contribute to hardness. At 700°C, in the

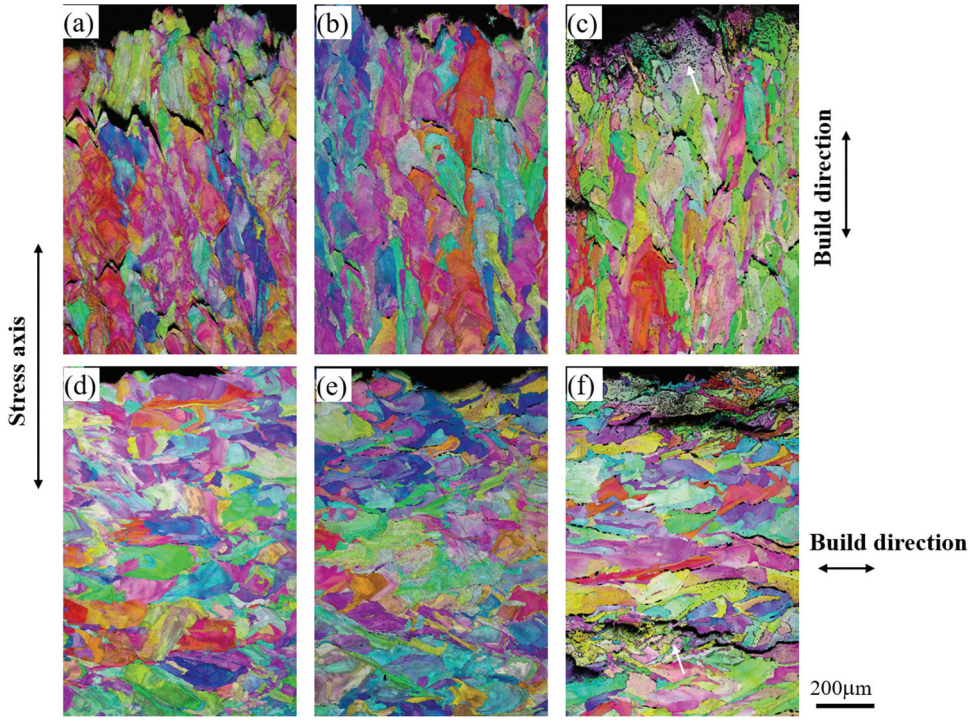

Figure 15. Inverse pole figure (IPF) map overlaid on the image quality (IQ) map by SEM-EBSD for creep ruptured specimens.(a)PiHA 700°C. 140MPa tr=5612.4h, (b) PiHA 800°C. 80MPa tr=4288.9h, (c) PiHA 900°C. 30MPa tr=5319.3h, (d) PiHC 700°C. 120MPa tr=4030.2h, (e) PiHC 800°C. 60MPa tr=903.8h, (f) PiHA 900°C. 15MPa tr=2949.5h. Arrows in(c) and (f) indicate Cr and O rich particles..

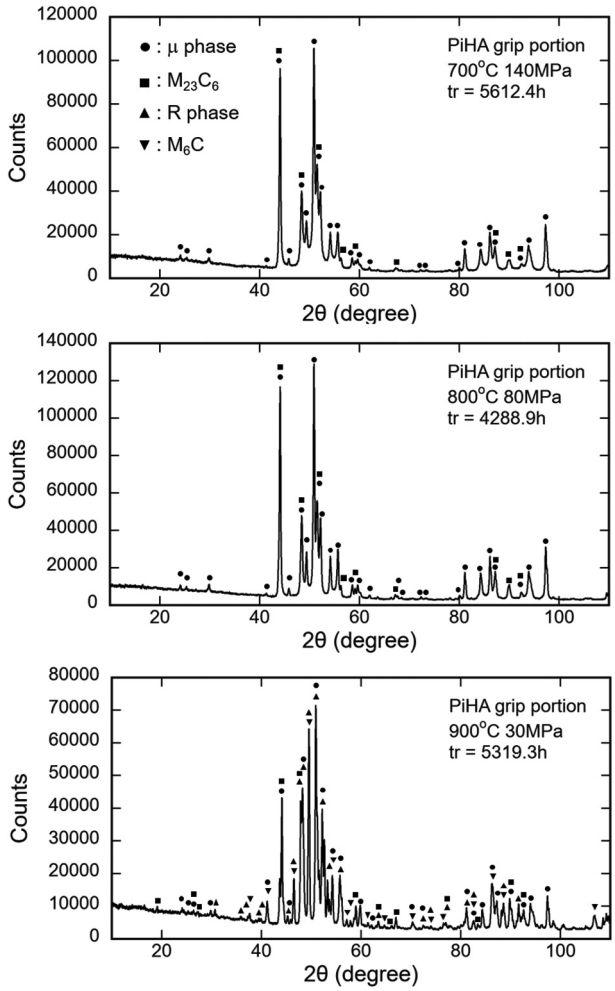

Figure 16. XRD results of extracted residue of grip portion of creep ruptured specimens for PiHA.

grip portion, the dislocations introduced by the AM process will not recover after creep exposure while precipitation can occur during creep exposure as shown in Figure 17. Therefore, the high hardness value is attributed to precipitation at 700°C. At 800°C and 900°C, the hardness of the grip portion decreased after creep rupture regardless of precipitation. In this case, dislocations introduced by the AM process may recover during aging even for the grip portion due to the high temperature. The hardness was basically higher in the grip portion than in the gauge portion after creep rupture. In the gauge portion, creep deformation can promote coarsening of precipitates, indicating a decrease in hardness.

4. Conclusions

Tensile and creep properties of Hastelloy X fabricated by laser powder bed fusion were obtained at 700°C to 1000°C. The 0.2% proof stress and tensile strength of PiHA and PiHC were basically equal to or higher than that of the conventional Hastelloy X although the tensile strength was slightly lower in PiHC than in the conventional Hastelloy X. On the other hand, the tensile ductility of PiHA and PiHC was much lower than that of the conventional Hastelloy X at 700°C to 1000°C. The creep strength of PiHA was similar to that of the conventional Hastelloy X while the creep life of PiHC was one order of magnitude shorter than that of the conventional one. The creep ductility was much lower in PiHA and PiHC than in the

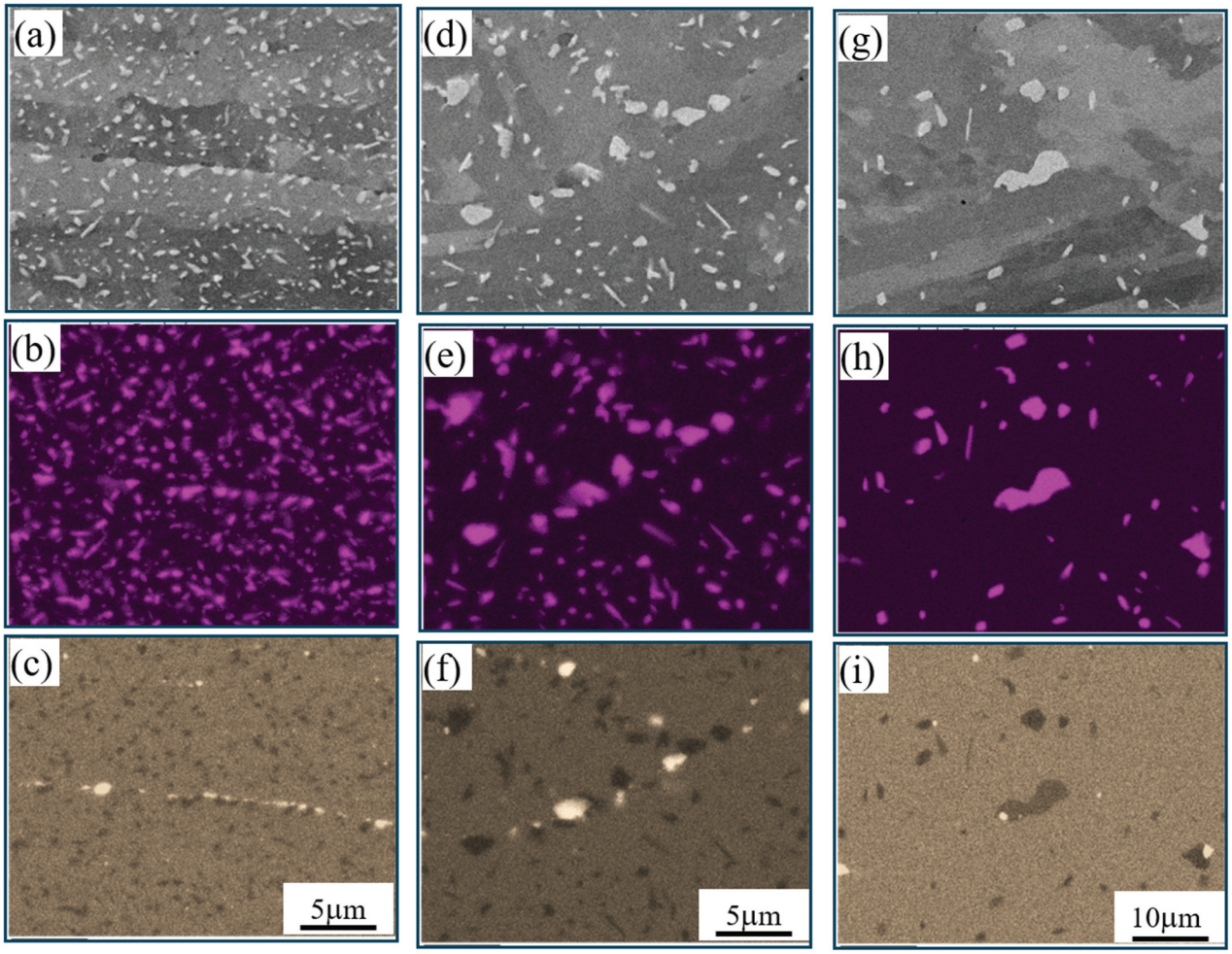

Figure 17. Results of elemental mapping by SEM-EDS for gauge portion of creep ruptured specimens of PiHA. (a)-(c)PiHA 700°C . 140MPa tr=5612.4h, (d)-(f)PiHA 800°C . 80MPa tr=4288.9h, (g)-(i)PiHA 900°C . 30MPa tr=5319.3h (a)(d)(g) SE image, (b)(e)(h) Mo map, (c)(f)(i) Cr map.

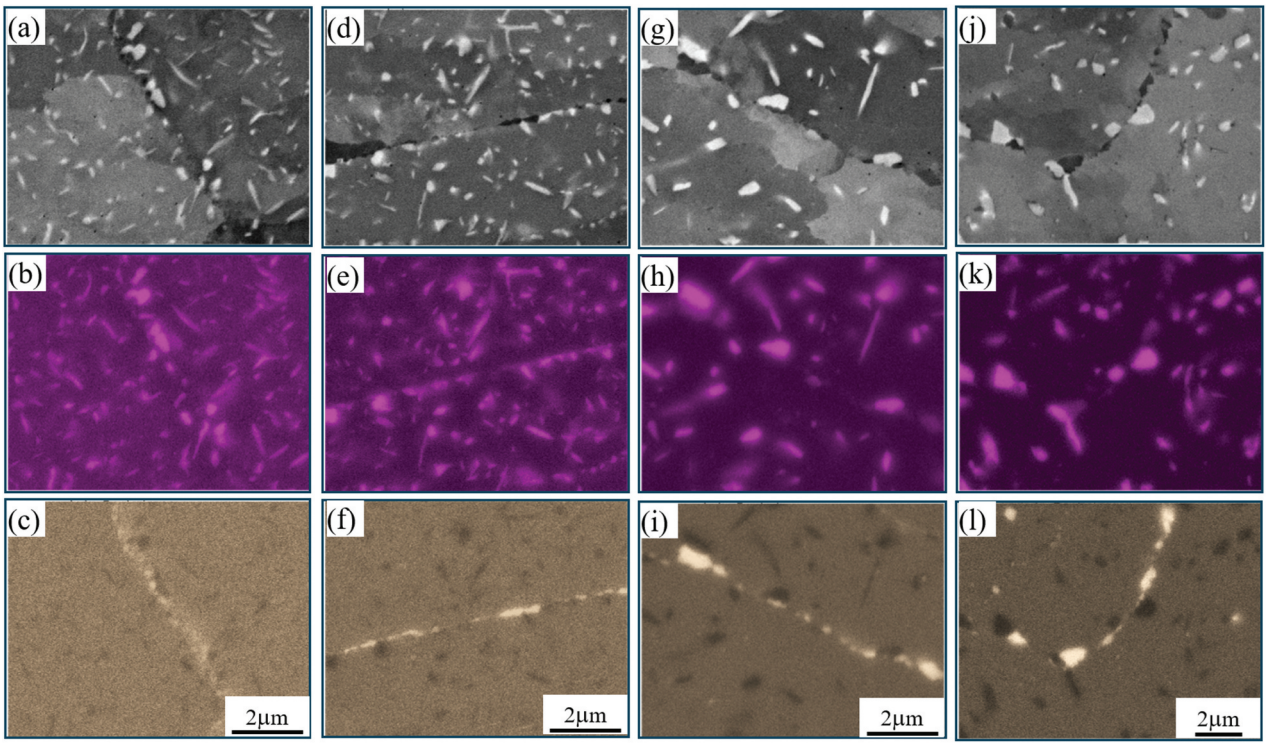

Figure 18. Results of elemental mapping by SEM-EDS for grip portion of creep ruptured specimens of PiHA. (a)-(c)PiHA 700°C 200MPa tr = 279.8h, (d)-(f)PiHA 700°C 180MPa tr = 680.8h, (g)-(i)PiHA 800°C 120MPa tr = 63.6h, (a)(d)(g)(j) SE image, (b)(e)(h)(k) Mo map, (c)(f)(i)(l)Cr map.

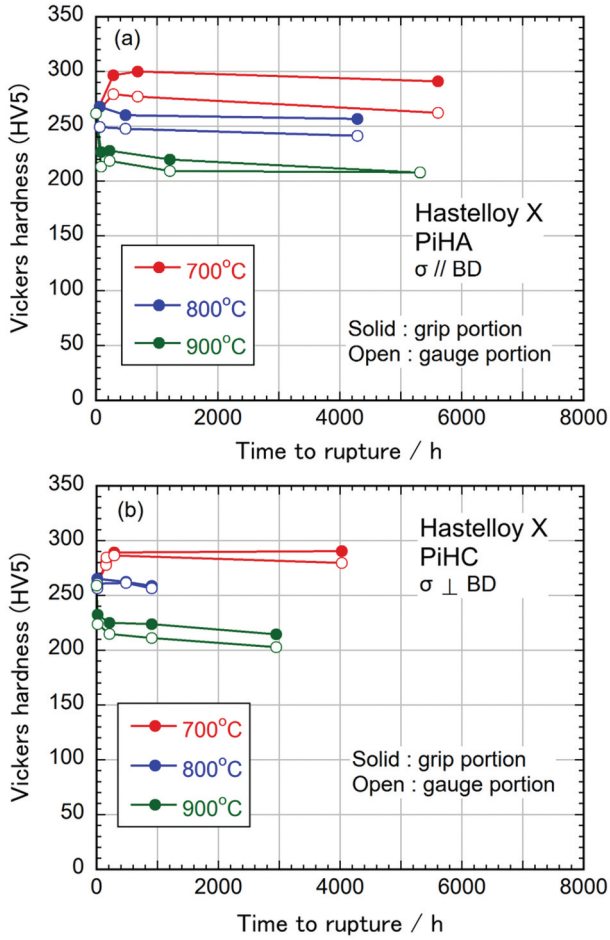

Figure 19. Vickers hardness of grip and gauge portion of creep ruptured specimens for (a) PiHA (b) PiHC. σ :stress axis BD:build direction

conventional Hastelloy X. For PiHA and PiHC, double local minimum values of creep rate were observed in creep rate versus time curves at 700°C and 800°C. $M_{23}C_6$, μ phase, R phase and M_6C particles were observed after creep exposure. The formation of these particles during creep exposure is proposed as a possible reason for the double local minimum values of creep rate. For estimating allowable stress of AM Hastelloy X, the creep strength of PiHC will be minimum value. Therefore, the creep strength of PiHC should be improved to establish allowable stress comparable to conventional Hastelloy X. It may be easy to use AM Hastelloy X for actual components when stress direction is not perpendicular to build direction in the actual components.

Acknowledgements

The authors thank Mr. Yasushi Taniuchi, Dr. Kaoru Sekido, and Mr. Takehiro Nojima for their support with creep testing (all at NIMS). This work was partly supported by a grant from the Amada Foundation (No. AF-2022201-A3).

Disclosure statement

No potential conflict of interest was reported by the author(s).

Funding

The work was supported by the Amada Foundation [AF-2022201-A3.

References

[1] Tang T Y, Panwisawas C, Ghoussoub N J, et al. Alloys-by-design: application to new superalloys for additive manufacturing. Acta Mater. 2021;202:417–436.

[2] Kalyanasundaram V, De Luca A, Wróbel R, et al. Tensile and creep-rupture response of additively manufactured nickel-based superalloy CM247LC. Addit Manuf Lett. 2023;5:100119. doi: 10.1016/j.addlet.2022.100119

[3] Kuo Y-L, Horikawa S, Kakehi K. Effects of build direction and heat treatment on creep properties of Ni-base superalloy built up by additive manufacturing. Scr Mater. 2017;129:74–78. doi: 10.1016/j.scriptamat.2016.10.035

[4] Sanchez S, Gaspard G, Hydea CJ, et al. The creep behaviour of nickel alloy 718 manufactured by laser powder bed fusion. Mater Des. 2021;204:109647.

[5] Pröbstle M, Neumeier S, Hopfenmüller J, et al. Superior creep strength of a nickel-based superalloy produced by selective laser melting. Mater Sci Eng A. 2016;674:299–307. doi: 10.1016/j.msea.2016.07.061

[6] Bürger D, Parsa AB, Ramsperger M, et al. Creep properties of single crystal Ni-base superalloys (SX): a comparison between conventionally cast and additive manufactured CMSX-4 materials. Mater Sci Eng A. 2019;762:138098. doi: 10.1016/j.msea.2019.138098
[7] El-Atwani O, Eftink BP, Cady CM, et al. Enhanced mechanical properties of additive manufactured grade 91 steel. Scr Mater. 2021;199:113888. doi: 10.1016/j.scriptamat.2021.113888
[8] Hatakeyama T, Sawada K, Kusano M, et al. Significant creep-strength improvement in modified 9Cr-1Mo steel via microstructural control through laser powder bed fusion. Addit Manuf. 2024;93:104445. doi: 10.1016/j.addma.2024.104445
[9] Li Y, T K, Podaný P, et al. Thermal stability of dislocation structure and its effect on creep property in austenitic 316L stainless steel manufactured by directed energy deposition. Mater Sci Eng A. 2019;873:144981.
[10] Yu JM, Dao VH, Yoon KB. Investigation of creep behavior of 316L stainless steel produced by selective laser melting with various processing parameters. J Mech Sci Tech. 2020;34(8):3249–3259. doi: 10.1007/s12206-020-0717-z
[11] Argonne National Lab. Anl-ammt-009. ASME code qualification plan for LPBF 316. SS; 2023.
[12] NRA Technical Note Series. Review of the current status of the development of advanced manufacturing technologies and their application in the nuclear fied. NTEN-2024–1001; 2024.
[13] American Society of Mechanical Engineers (ASME). Asme boiler and pressure vessel code. Section ii. Part D. 2023.
[14] Megahed S, M KK, Heinze C, et al. Influence of build orientation on the creep behavior of IN738LC manufactured with laser powder bed fusion. Mater Sci Eng A. 2023;878:145197.
[15] Yoshioka Y, Saito D, Fujiyama K, et al. Effect of microstructure on creep resistance of Hastelloy X. Tetsu-To-Hagane. 1994;80(10):789–794. doi: 10.2355/tetsutohagane1955.80.10_789
[16] Agrawal S, Kumar C, Avadhani GS, et al. Anisotropic creep and stress rupture behaviour of laser powder bed fusion processed Hastelloy X. Mater Sci Eng A. 2025;934:148342. doi: 10.1016/j.msea.2025.148342
[17] Wu S, Dai SB, Heilmaier M, et al. The effect of carbides on the creep performance of Hastelloy X fabricated by laser powder bed fusion. Mater Sci Eng A. 2023;875:145116. doi: 10.1016/j.msea.2023.145116
[18] Poggio E, Allen DJ, Barnard P, et al. ECCC working group 3C – Superalloys overview on the activities and future perspectives. In: Barnard P, editor. Proceedings of 6th International Creep & Fracture Conference; Edinburgh. European Creep Collaborative Committee; 2023; May 22–24. p. 440–450.
[19] Japanese industrial standards (JIS). Method of elevated temperature tensile test for steels and heat-resisting alloys. 1998. (JIS G 0567;).
[20] Japanese industrial standards (JIS). Method of creep and creep rupture test for metallic materials. JIS Z. 2271; 1998.
[21] Sawada K, Taniuchi Y, Sekido K, et al. Long-term creep properties of Ni-based 21Cr-18Fe-9Mo superalloys. Sci Tech Adv Mater. 2023;3(1):2284129. doi: 10.1080/27660400.2023.2284129
[22] Sanchez-Mata O, Muñiz-Lerma JA, Wang X, et al. Microstructure and mechanical properties at room and elevated temperature of crack-free Hastelloy X fabricated by laser powder bed fusion. Mater Sci Eng A. 2020;780:139177. doi: 10.1016/j.msea.2020.139177
[23] National Institute for Materials Science. NIMS creep data sheet No.55A. NIMS; 2023.
[24] Hatakeyama T, Sawada K, Sekido K, et al. Influence of dynamic microstructural changes on the complex creep deformation behavior of 25Cr–20Ni–Nb–N steel at 873 K. Mater Sci Eng A. 2021;814:141270. doi: 10.1016/j.msea.2021.141270
[25] Karapuzha AS, Fraser D, Schliephake D, et al. Room and elevated temperature tensile and fatigue behaviour of additively manufactured Hastelloy X. Mater Sci Eng A. 2023;882:145479. doi: 10.1016/j.msea.2023.145479
[26] Sawada K, Hatakeyama T, Sekido K, et al. Microstructural changes and creep-strength degradation in 18Cr-9Ni-3Cu-Nb-N steel. Mater Charact. 2021;178:111286. doi: 10.1016/j.matchar.2021.111286
[27] Agrawal S, Avadhani GS, Suwas S. Evolution of new topologically close-packed phases P and R upon long-term isothermal aging of laser powder bed fusion processed Hastelloy X. J Alloys Comp. 2025;1010:177597. doi: 10.1016/j.jallcom.2024.177597
[28] Kimura K, Sawada K. Creep deformation property and creep life evaluation of Super304H. J. Press. Vessel Tech. 2022;144(2):021507. doi: 10.1115/1.4052397
[29] Hatakeyama T, Sawada K, Sekido K, et al. Beneficial role of the grain boundary precipitates for intergranular creep fracture of 25Cr–20Ni–Nb–N steel. Mater Sci Eng A. 2023;882:145487. doi: 10.1016/j.msea.2023.145487
[30] Lin D, Hu J, Wu R, et al. Multiscale plastic deformation in additively manufactured FeCoCrNiMox high-entropy alloys to achieve strength–ductility synergy at elevated temperatures. Int J Plasticity. 2024;183:104142.